

Homework 4

Field and Service Robotics

Lorenzo Palma Xu
P38000303

June 2025

Contents

- Exercise 1	3
- Exercise 2	3
- Exercise 3	4
- Exercise 4	14

Exercise 1

- Buoyancy Effect

The *Buoyancy Effect* or *Archimedes' Principle* is an hydrostatic effect considered when a rigid body is submerged in a fluid under the effect of gravity.

The Buoyancy is defined as:

$$b = \rho\Delta||\bar{g}||$$

where

$$\bar{g} = [0 \ 0 \ 0]^T$$

$g \in \mathbb{R}$, the gravity acceleration

$\Delta \in \mathbb{R}$, the volume of the body

$\rho \in \mathbb{R}$, the density of the water

Considering the center of mass of the underwater robot, $r_c^b \in \mathbb{R}^3$, it's possible to write the vector of the gravity force as:

$$f_g^b = R_b^T \begin{bmatrix} 0 \\ 0 \\ w \end{bmatrix} = R_b^T \begin{bmatrix} 0 \\ 0 \\ mg \end{bmatrix}$$

with w the submerged weight of the body, and $m \in \mathbb{R}$ the mass of the body

and the buoyancy force, that acts at the center of buoyancy $r_b^b \in \mathbb{R}^3$ equal to:

$$f_b^b = -R_b^T \begin{bmatrix} 0 \\ 0 \\ b \end{bmatrix} = -R_b^T \begin{bmatrix} 0 \\ 0 \\ \rho\Delta g \end{bmatrix}$$

where the minus sign indicates that this effect (upward) is opposite to the gravitational force (downward).

This two effects provide a wrench, that in the body-fixed frame is:

$$g_{rb}^b = - \begin{bmatrix} f_g^b + f_b^b \\ S(r_c^b)f_g^b + S(r_b^b)f_b^b \end{bmatrix} \in \mathbb{R}^6$$

The first torque term vanishes when the reference frame is centered at the center of mass, whereas the second term vanishes if the frame is placed at the center of buoyancy.

Looking at the Buoyancy formula, a crucial factor is the density of the fluid. For example, water has a density of approximately $\rho_{water} \simeq 1000 \text{ kg/m}^3$, while for the air is about $\rho_{air} \simeq 1.2 \text{ kg/m}^3$. For this reason, in aerial robotics this effect is typically neglected, as the air density is much lower than the density of the moving mechanical system. In contrast, in underwater robotics, the density of the water is comparable to that of the robot, and also the volume of displaced fluid is significant, making the buoyancy effect non-negligible.

Exercise 2

- a. False

The *Added Mass Effect* in underwater robotics, doesn't represent a physical quantity of fluid to be added to the system, like an additional load, but rather an inertial effect caused by the surrounding fluid being accelerated along with the body. This results in a dynamic resistance equivalent to an increase in the system's effective mass, known as added mass or virtual mass.

From a dynamics perspective, the fluid exerts a reaction force equal in magnitude and opposite in direction to the acceleration imposed by the robot in accordance with Newton's third law. This reaction contributes to the total inertia of the system and is accounted for in the equations of motion.

- b. True

As explained in the previous exercise, the density of water is approximately 833 times greater than that of air. For this reason, it is comparable to the density of the mechanical system in motion, and it cannot be neglected, unlike in aerial robotics, where the air density is much lower than that of the robot.

- c. True

The *Damping Effect* accounts for the presence of dissipative drag and lift forces acting on the body, due to the viscosity of the surrounding fluid. This viscous effect results from the combination of these two forces:

- the drag force, which acts parallel to the relative velocity between the body and the fluid;
- the lift force, which acts perpendicular to the drag.

Damping is typically modeled using only quadratic terms with constant coefficients, grouped into the damping matrix $D_{RB} \in \mathbb{R}^{6 \times 6}$, which is positive definite. This matrix captures the nonlinear nature of hydrodynamic resistance at higher velocities.

The damping effect plays an important role in stability analysis, as it contributes to energy dissipation in the system, helping to reduce oscillations and prevent sustained or increasing motion over time.

- d. False

The *Current Effect*, which accounts for environmental disturbances such as waves, wind and ocean current, is typically assumed to be constant and irrotational only when expressed in the world or Earth-fixed frame. It cannot be considered constant if expressed in the body frame, as this frame moves and rotates with the vehicle, causing the current to appear time-varying. This would make modeling and control more complex and less intuitive.

The Ocean current expressed in the world frame is:

$$v_c = \begin{bmatrix} v_{c,x} \\ v_{c,y} \\ v_{c,z} \\ 0 \\ 0 \\ 0 \end{bmatrix} \in \mathbb{R}^6 \quad \dot{v}_c = 0^6$$

But can also be expressed in the body-fixed frame considering the relative velocity :

$$v_r = \begin{bmatrix} \dot{p}_b^b \\ \omega_b^b \end{bmatrix} - R_b^T v_c$$

Exercise 3

- a. Quadratic Problem

In order to control a quadruped robot, it is necessary a *Whole-Body Controller*, that decouples the motion planning from the control.

This controller is contained in the file `quadruped_simulation.zip`.

To solve the following quadratic problem:

$$\begin{aligned} \min_x \quad & \frac{1}{2} x^\top H x + g^\top x \\ \text{s.t.} \quad & A_{\text{ineq}} x \leq b_{\text{ineq}} \\ & A_{\text{eq}} x = b_{\text{eq}} \end{aligned}$$

The QPsolver qpSWIFT has been used, which is described in the file `qpSWIFT.m`, through the line:

```
[sol] = qpSWIFT(sparse(H),g,sparse(Aeq),beq,sparse(Aineq),bineq)
```

- b. Simulation

For the simulation, the gaits will be considered as distinct movement patterns, and the differences between them will be evaluated by varying several parameters such as desired velocity, friction coefficient, and the robot's mass.

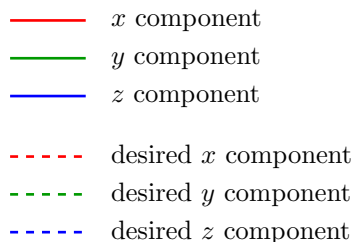
The videos of the simulations have been uploaded at the following link:

https://github.com/Pixel-0-1/Homework_4_FSR_24-25.git

The list of gaits is as follows:

- 0 - **Trot**: A symmetrical, stable, and fairly fast gait in which diagonal pairs of legs move together (as in horses).
- 1 - **Bound**: A gait in which the front and rear legs move in synchronized pairs (as in rabbits).
- 2 - **Pacing**: A lateral gait in which the legs on the same side of the body move together (as in camels).
- 3 - **Gallop**: The fastest and most asymmetrical gait, where at certain moments all four legs may be off the ground (as in cheetahs).
- 4 - **Trot Run**: A gait between a trot and a gallop, often observed in agile animals (as in cats).
- 5 - **Crawl**: A slow and stable gait in which each leg moves one at a time. It is especially used on rough terrain to maximize balance and stability (as in turtles).

The legend used is the following:



For the z-component of the ground reaction forces, the four different colors represent the four legs of the quadruped robot.

Gait 0 - Trot

Figure 1 shows the behavior of the quadruped robot with the default settings. We can observe that it reaches 2 meters along the axes-x after 4.5 seconds, and the desired velocity in approximately 1 second. The robot exhibits stable and well-controlled trotting with accurate velocity tracking, symmetric ground reaction forces, and expected angular velocity oscillations.

In Figure 2, we can observe a backward movement, with the desired velocity along the x-axes $v_d = -0.4$ m/s. Although the robot shows initial instability during the first second, after reaching the desired velocity, it quickly recovers and successfully completes the backward trotting motion. This might represent the limit of tolerable backward velocity, as higher negative values would lead to excessive instability and unrealistic motions that the robot would not be able to perform in real-world conditions.

Figure 3 shows the case of an increased desired velocity $v_d = 1.5$ m/s. as the velocity increases, the robot's behavior deteriorates: although it reaches the desired speed after approximately 3 seconds, it exhibits unstable motion while trying to maintain it. This value can be considered an the upper limit for feasible motion.

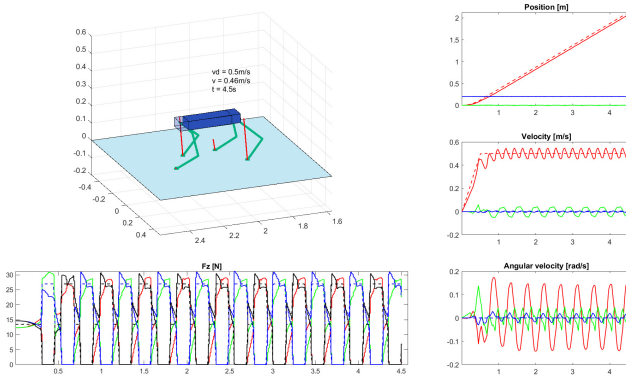


Figure 1: Trot with default settings: $m = 5.5 \text{ kg}$, $v_d = 0.5 \text{ m/s}$, $\mu = 1$

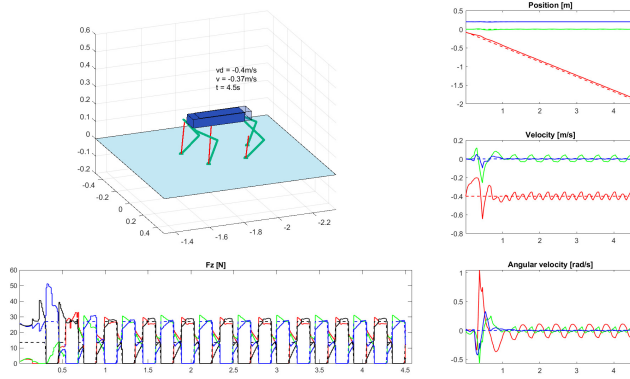


Figure 2: Trot with negative desired velocity: $m = 5.5 \text{ kg}$, $v_d = -0.5 \text{ m/s}$, $\mu = 1$

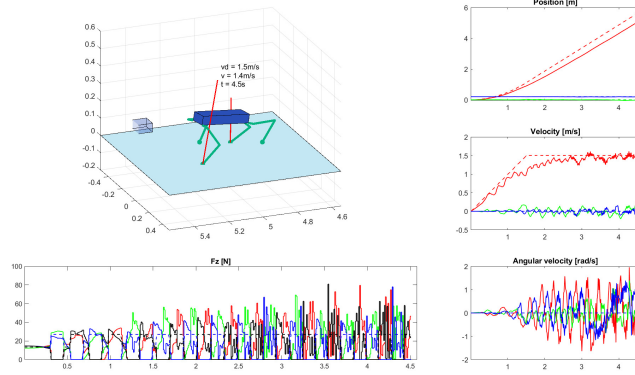


Figure 3: Trot with positive desired velocity: $m = 5.5 \text{ kg}$, $v_d = 1.5 \text{ m/s}$, $\mu = 1$

In Figure 4 we can observe the simulation with a lower mass, $m = 1 \text{ kg}$ that only involves in a reduction of the oscillation, specially for velocity, and lower peaks for the z-component of the ground reaction forces. (For heavier masses, it's exactly the opposite)

Finally in Figure 5, reducing the friction coefficient from 1.0 to 0.1 leads to noticeable peaks in angular velocity (up to $\pm 0.5 \text{ rad/s}$), while for linear velocity also the z-component oscillates. This

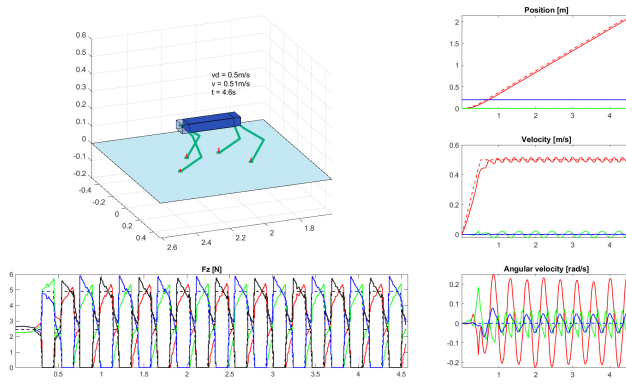


Figure 4: Trot with lower mass: $m = 1 \text{ kg}$, $v_d = 0.5 \text{ m/s}$, $\mu = 1$

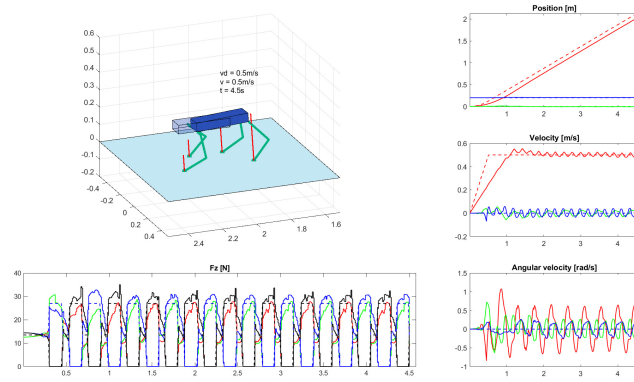


Figure 5: Trot with lower friction coefficient: $m = 5.5 \text{ kg}$, $v_d = 0.5 \text{ m/s}$, $\mu = 0.1$

is due to increased foot slippage, which reduces the robot's ability to control rotational dynamics, causing instability around the yaw axis.

Gait 1 - Bound

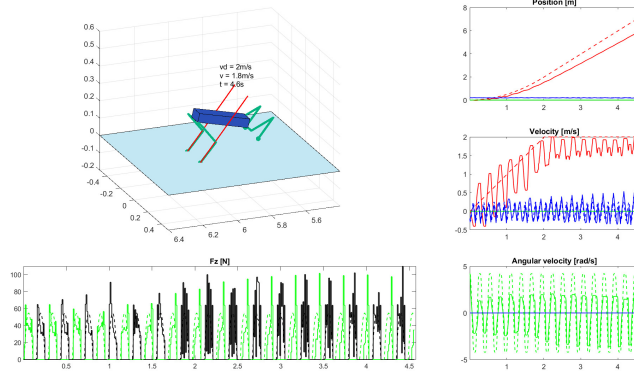


Figure 6: Bound with default settings: $m = 5.5 \text{ kg}$, $v_d = 2 \text{ m/s}$, $\mu = 1$

Figure 6 shows the default bound gait, where the robot reaches the desired forward velocity of 2 m/s in approximately 2 seconds, but with significant angular oscillations (up to ± 5 rad/s), indicating reduced stability. Although the foot contact forces exhibit a regular pattern, the robot shows signs of limited rotational control and delayed velocity tracking, especially during the initial phase.

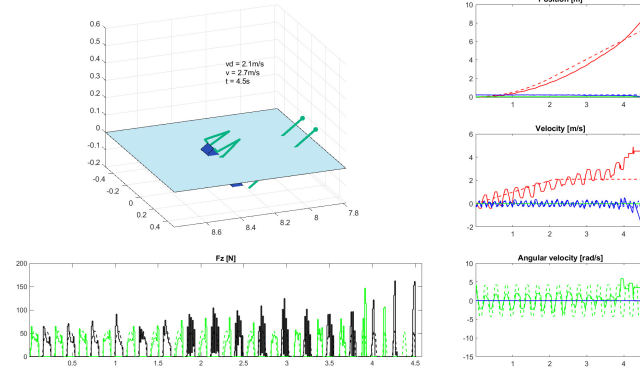


Figure 7: Bound with positive desired velocity: $m = 5.5$ kg, $v_d = 2.1$ m/s, $\mu = 1$

In Figure 7 we can observe that as for the case of the trot, for a greater velocity, the instability may cause the breaking of the robot, and this happens precisely with $v_d \geq 2.1$ m/s and $v_d \leq -1.5$ m/s.

Due to the fact that this gait is less stable than the trot, also a small increase of mass, causes the robot to fall, in fact, with $m = 6$ kg the behavior is similar to that of Figure 7, while for smaller values of mass, we have the same improvement of the trot.

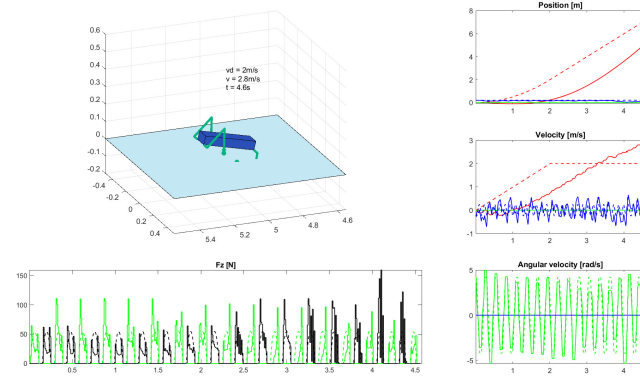


Figure 8: Bound with lower friction coefficient: $m = 5.5$ kg, $v_d = 2$ m/s, $\mu = 0.1$

Finally in Figure 8 the friction coefficient was reduced to 0.1, leading to poorer tracking of the desired velocity and a noticeable delay in position.

Gait 2 - Pacing

The simulation of the pacing gait is shown in Figure 9, where we have great oscillation for angular velocity and also y-component of the linear velocity, due to the nature of this gait where the legs on the same side move together.

In Figure 10, there is the backward movement with the desired velocity $v_d = -0.6$ m/s. The robot shows initial instability during the first second, but after reaching the desired velocity, it recovers and completes the motion. As always, higher negative values would lead to excessive instability during the transient that the robot would not be able to perform in real-world.

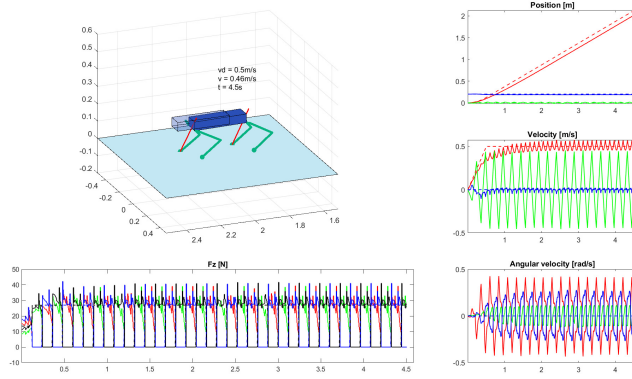


Figure 9: Pacing with default settings: $m = 5.5 \text{ kg}$, $v_d = 0.5 \text{ m/s}$, $\mu = 1$

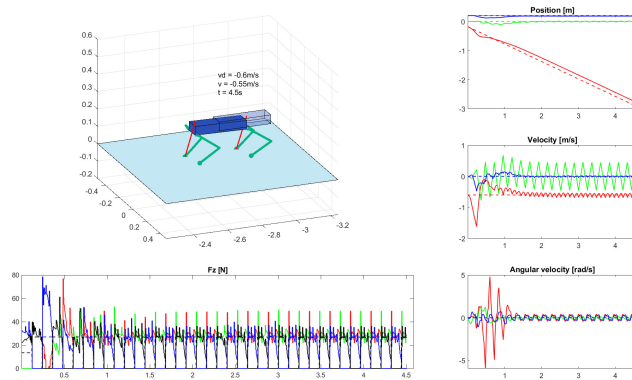


Figure 10: Pacing with negative desired velocity: $m = 5.5 \text{ kg}$, $v_d = -0.6 \text{ m/s}$, $\mu = 1$

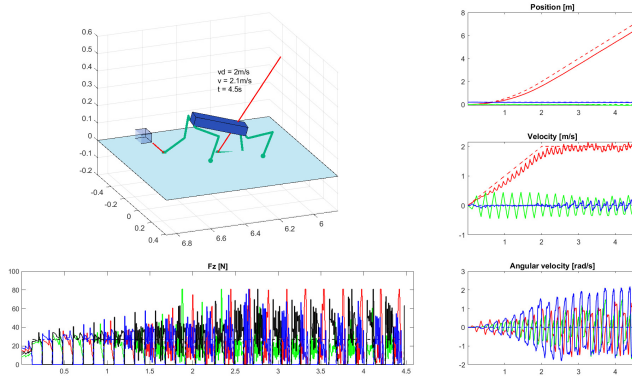


Figure 11: Pacing with positive desired velocity: $m = 5.5 \text{ kg}$, $v_d = 2 \text{ m/s}$, $\mu = 1$

Figure 11 illustrates that for velocities $v_d \geq 2 \text{ m/s}$, the system struggles to follow the desired position and maintain stability, primarily due to the substantial rise in angular velocity. For the usual mass of 1 kg (Figure 12), there is a clear improvement in position tracking, lower values of F_z , and reduced oscillations in v_x , ω_y , and ω_z . Conversely, as the mass increases, these aspects progressively worsen up to $m = 10 \text{ kg}$, after which the system becomes so unstable that

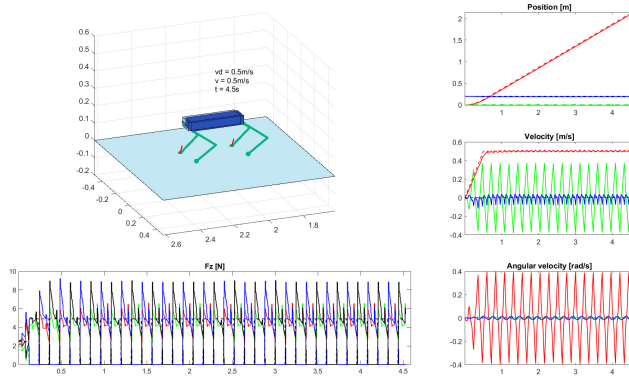


Figure 12: Pacing with lower mass: $m = 1 \text{ kg}$, $v_d = 0.5 \text{ m/s}$, $\mu = 1$

the quadruped could potentially break.

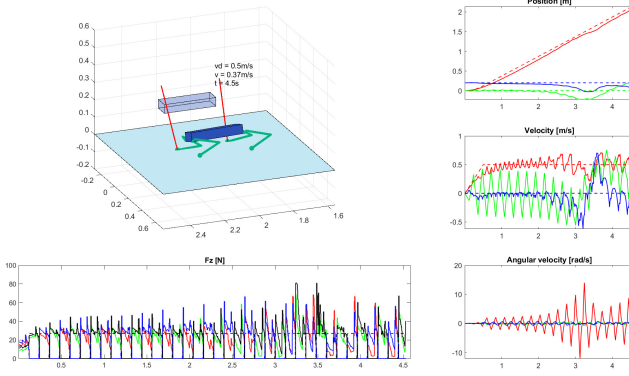


Figure 13: Pacing with lower friction coefficient: $m = 5.5 \text{ kg}$, $v_d = 0.5 \text{ m/s}$, $\mu = 0.7$

From Figure 13, it can be observed that in this case, a friction coefficient $\mu \leq 0.7$ is sufficient to reduce stability to the point where the robot is no longer able to maintain its desired position along the y and z axes, even penetrating the floor.

Gait 3 - Gallop

Figure 14 displays the gallop with the default settings. Although it should be the fastest gait, a big oscillation around the desired velocity, especially for the x -component, makes the robot cover approximately 2 meters. The z -component of the ground reaction forces is high as the bound gait.

When the desired linear velocity is $v_d \geq 1 \text{ m/s}$, the angular velocity increases such that the direction of the motion, is no longer translational, but diagonal. The lower bound for negative velocities that allow the quadruped to restore the control, is $v_d = -0.7 \text{ m/s}$.

For lower mass, like $m = 1 \text{ kg}$, there is the usual improvement for v_x and F_z , while for an higher mass $m = 15 \text{ kg}$, F_z doubles and the angular velocity quadruples, causing a large offset for the x and y position. (Figure 16)

For a lower friction coefficient instead, we have a behavior similar to the higher mass, where the quadruped robot rotate around the z -axis due to the increment of the angular velocity, but the oscillation in position and linear velocity slightly decreases.

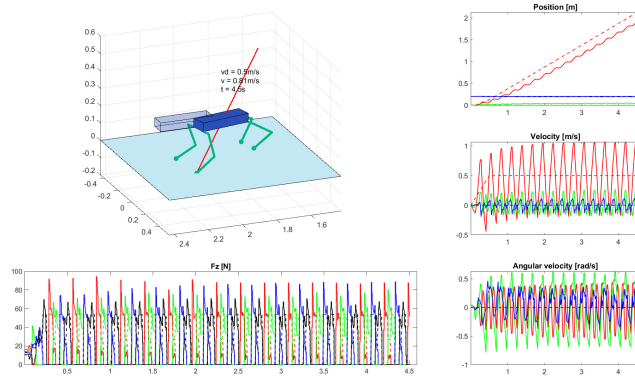


Figure 14: Gallop with default settings: $m = 5.5 \text{ kg}$, $v_d = 0.5 \text{ m/s}$, $\mu = 1$

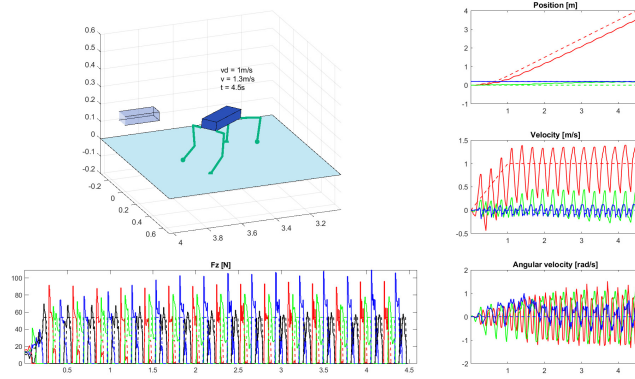


Figure 15: Gallop with positive desired velocity: $m = 5.5 \text{ kg}$, $v_d = 1 \text{ m/s}$, $\mu = 1$

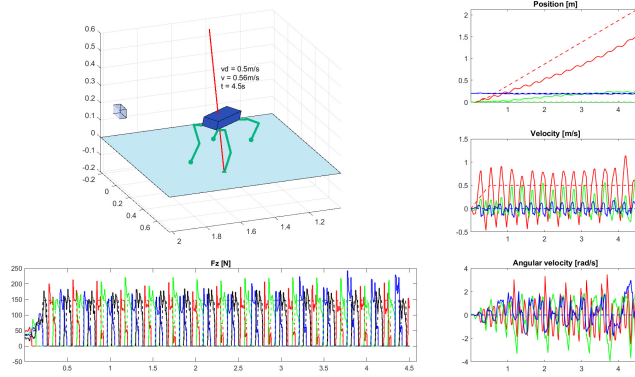


Figure 16: Gallop with higher mass: $m = 15 \text{ kg}$, $v_d = 0.5 \text{ m/s}$, $\mu = 1$

Gait 4 - Trot Run

For the gait 4, comparing the Figure 17 with respect to the gait 0 (Figure 1), it's clear that the oscillation for v_x decreases, but on the other side the one for v_y and v_z increases. The same happens with the angular velocity, and also the F_z is bigger.

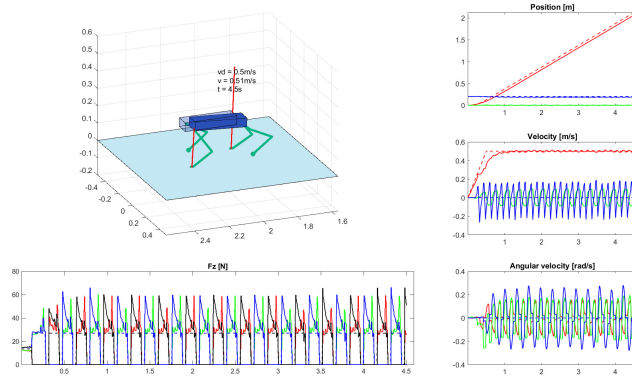


Figure 17: Trot Run with default settings: $m = 5.5 \text{ kg}$, $v_d = 0.5 \text{ m/s}$, $\mu = 1$

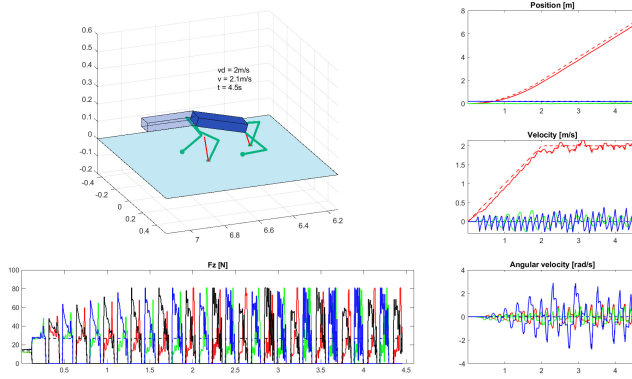


Figure 18: Trot Run with positive desired velocity: $m = 5.5 \text{ kg}$, $v_d = 2 \text{ m/s}$, $\mu = 1$

This time the lower bound for negative velocities is $v_d = -0.5 \text{ m/s}$, that is the limit to which the robot still succeeds the motion, while for positive velocities is $v_d = 2 \text{ m/s}$ (Figure 18), higher speeds may be not feasible, causing the robot to break.

For a mass $m = 1 \text{ kg}$ there is only a little improvement of the y-component of the angular velocity and a less F_z (approximately a quarter), while for a mass $m = 15 \text{ kg}$ both F_z and ω_z double.

With a friction coefficient of $\mu = 0.1$, the behavior is very similar to the default simulation, with a slight increase in the oscillations of the x-component for both linear and angular velocities.

Gait 5 - Crawl

The robot exhibits in Figure 19 stable and controlled locomotion using a crawl gait. The position and velocity tracking are accurate, the forces are well-distributed, and the angular motion remains within acceptable bounds. This gait appears effective for low-speed movement with a strong focus on balance and stability.

In figure 20 we can observe that the tracking is really accurate also for higher velocity, like $v_d = 2.5 \text{ m/s}$ despite the increase of ω and F_z . Vice versa, for negative velocity, the limit is lower w.r.t. all the previous gaits, in fact the lower limit is only $v_d = -0.3 \text{ m/s}$, beyond this limit, the robot risks breaking.

A smaller mass $m = 1 \text{ kg}$, this time, involves a notable improvement, as we can see in Figure 21, especially for the linear velocity and for the reaction forces. An increment of the mass (e.g. $m = 15$

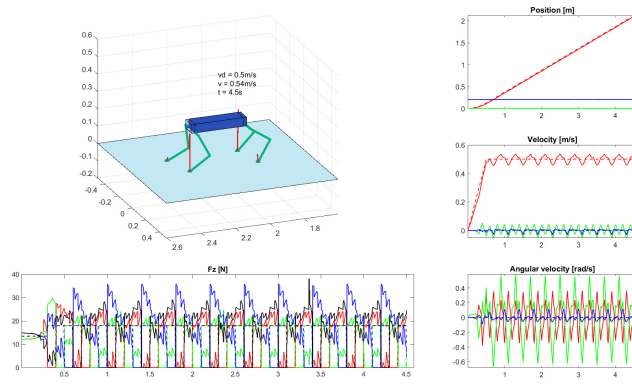


Figure 19: Crawl with default settings: $m = 5.5 \text{ kg}$, $v_d = 0.5 \text{ m/s}$, $\mu = 1$

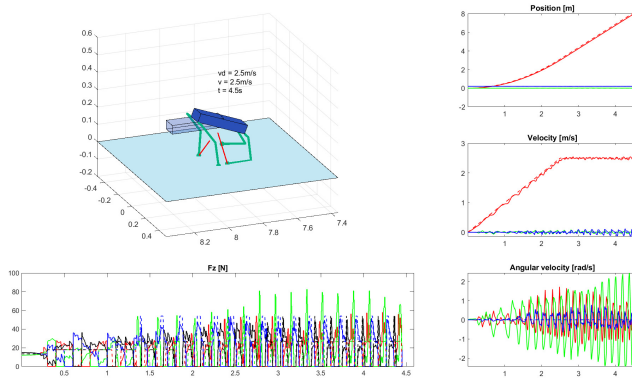


Figure 20: Crawl with positive desired velocity: $m = 5.5 \text{ kg}$, $v_d = 2.5 \text{ m/s}$, $\mu = 1$

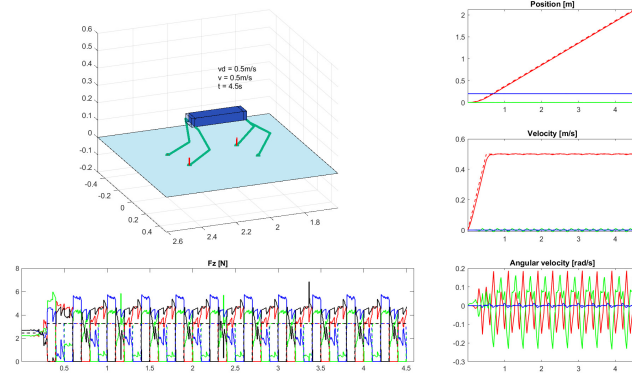


Figure 21: Crawl with lower mass: $m = 1 \text{ kg}$, $v_d = 0.5 \text{ m/s}$, $\mu = 1$

kg), as usual brings the opposite result.

Finally the last case, is when the friction coefficient is $\mu = 0.1$. In this case the behavior is almost identical to that with the default values, except for the x-component of the angular velocity, which equals the y-component.

Exercise 4

- Rimless Wheel

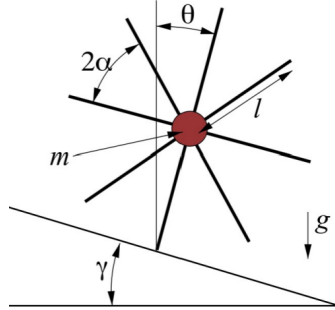


Figure 22: Rimless Wheel

It's the simplest possible model of a legged robot, constituted by rigid legs and a single point mass at the hip.

To study the model in Figure 22, four different assumptions will be considered:

1. Collisions with ground are inelastic and impulsive.
2. The stance foot acts as a pin joint and does not slip.
3. The transfer support at the time of contact is instantaneous.
4. $0 \leq \gamma < \frac{\pi}{2}$, $0 < \alpha < \frac{\pi}{2}$, $l > 0$

When a leg is on the ground, the dynamic is ruled by the simple pendulum equation:

$$\ddot{\theta} = \frac{g}{l} \sin \theta$$

For the forwarding walking, starting from a configuration $\theta(0^+) = \gamma - a$, the system needs an initial velocity $\dot{\theta}(0^+) > \omega_1$, where this threshold is:

$$\omega_1 = \sqrt{2 \frac{g}{l} (1 - \cos(\gamma - \alpha))}$$

This represents the minimum kinetic energy needed to make the mass climb over the supporting leg and take a step.

- If $\gamma = \alpha$, the configuration is symmetric and $\omega = 0$.
- If $\gamma > \alpha$, the mass is ahead of the stance foot, so the equilibrium point disappear and ω doesn't exist.

The next foot touches the ground when $\theta(t) = \gamma \pm a$, and the potential energy converts into kinetic energy with speed:

$$\dot{\theta}(t^-) = \sqrt{\dot{\theta}^2(0^+) + 4 \frac{g}{l} \sin \alpha \sin \gamma}$$

Therefore, with this model, the wheel starts rolling; then either it runs out of energy and stops, or rapidly converges to a stable periodic solution.

a. Simulation modifying the initial angular velocity

Figure 23 shows the results of the simulation with $\dot{\theta}_0 = 0.95$ rad/s. In the time history plot, we can observe a transient phase for the state trajectories θ and $\dot{\theta}$, with oscillations fading out in approximately 3 seconds, indicating that the system has reached a steady-state behavior. In the phase portrait, the presence of inward spiraling trajectory indicates that the system converges to a single stable equilibrium point.

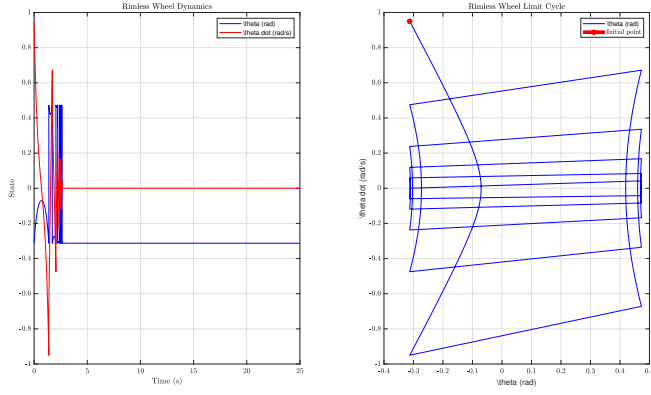


Figure 23: Time History (left) and Phase Portrait (right) with $\dot{\theta}_0 = 0.95 \text{ rad/s}$

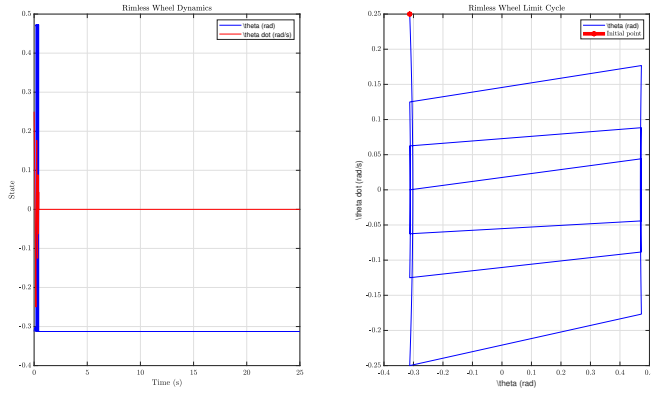


Figure 24: Time History (left) and Phase Portrait (right) with $\dot{\theta}_0 = 0.25 \text{ rad/s}$

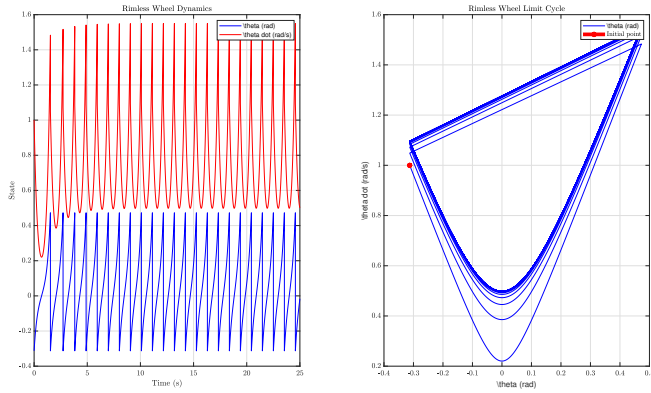


Figure 25: Time History (left) and Phase Portrait (right) with $\dot{\theta}_0 = 1 \text{ rad/s}$

With the initial angular velocity set to 0.25 rad/s (Figure 24), the system again converges to the equilibrium point, but more quickly (approximately 0.5 seconds). For an initial angular velocity of 1 rad/s (Figure 25) the system instead enters into a stable limit cycle, as indicated by the periodic trajectory shown in the phase portrait.

Therefore, initial conditions with low positive angular velocity (up to precisely 0.97), lie within the

basin of attraction of a stable equilibrium, where the wheel lacks the energy required for sustained walking. On the other hand, for $\dot{\theta}_0 \geq 0.98$, the system falls into the basin of attraction of the limit cycle, resulting in the perpetual rotation.

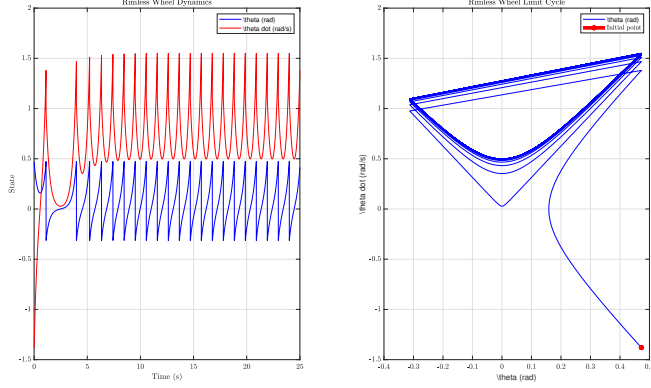


Figure 26: Time History (left) and Phase Portrait (right) with $\dot{\theta}_0 = -1.38 \text{ rad/s}$

For negative values, the threshold to reach the equilibrium point is higher: in fact, only for $\dot{\theta}_0 \leq -1.37$ does the system converge to an equilibrium point. For sufficiently large negative initial angular velocities (i.e., uphill motion on the inclined plane), the system initially slows down, but the gained potential energy causes the wheel to reverse direction and fall, ultimately converging to the same walking limit cycle as in the positive case (Figure 26).

b. Simulation modifying the leg length, the inter-leg length and slope inclination

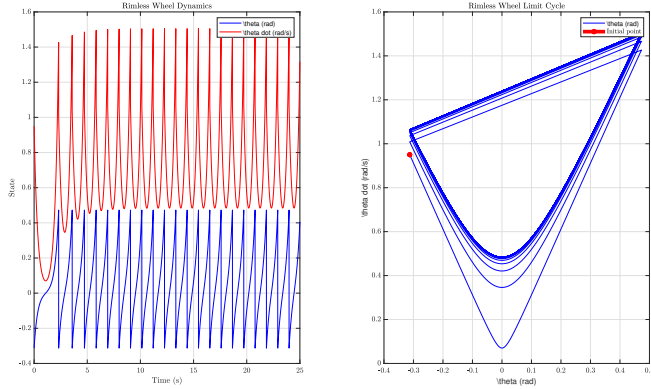


Figure 27: Time History (left) and Phase Portrait (right) with $l = 1.06 \text{ m}$

By changing the leg length of the rimless wheel, we observe that shorter legs lead to the wheel stopping more quickly, reaching the static equilibrium point. On the other hand, just a few extra centimeters are enough to push it into the rolling-induced limit cycle (in particular for $l \geq 1.06 \text{ m}$, as we can see in Figure 27).

When modifying the inter-leg angle, the effect is reversed: increasing the angle causes the wheel to stop sooner; decreasing the angle leads to a limit cycle. In Figure 28 where $\alpha = \frac{\pi}{16}$, the system evolves into a limit cycle shifted to a higher angular velocity.

Lastly, for the slope inclination, the results closely mirror those of the inter-leg angle. A gentler slope causes the wheel to stop sooner, while a steeper slope drives it into a limit cycle with increasingly high angular speed. Notably, increasing γ from $0.08 \rightarrow 0.09$ is enough to trigger a limit

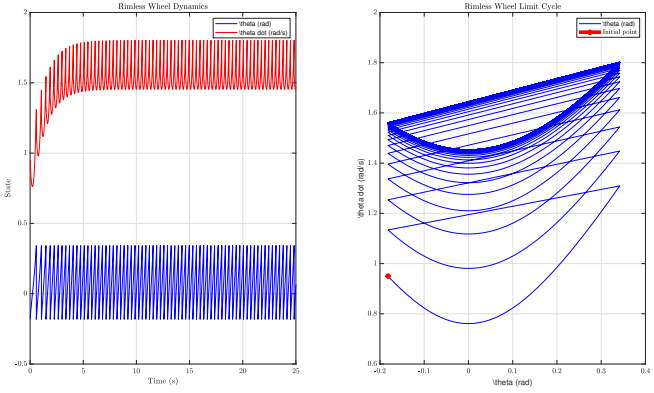


Figure 28: Time History (left) and Phase Portrait (right) with $\alpha = \frac{\pi}{16}$ rad

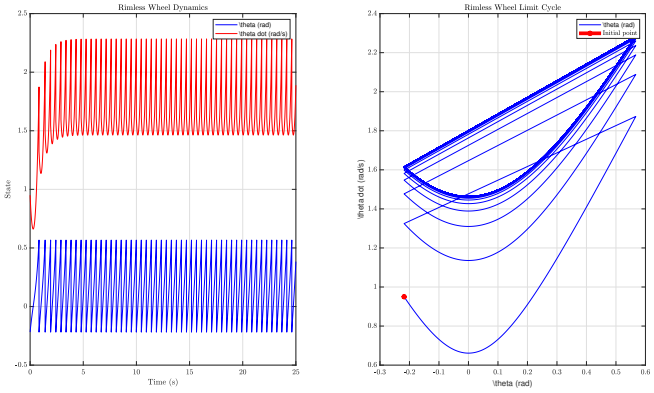


Figure 29: Time History (left) and Phase Portrait (right) with $\gamma = 0.17$ rad

cycle, and in the Figure 29 it is evident how the limit cycle shifts to higher angular velocities as the slope inclination γ increases.

From the simulations, it is evident that the rimless wheel exhibits both a stable equilibrium and a stable limit cycle, depending on the initial conditions and system parameters. The angular velocity threshold separating the two basins of attraction lies around $\dot{\theta}_0 \approx 0.97$ rad/s for positive values, and a more negative threshold for the uphill case.

Parameter variations reveal that the system's dynamics are highly sensitive to leg length, inter-leg angle, and slope inclination. Longer legs, smaller inter-leg angles, or steeper slopes tend to favor limit cycles (i.e., sustained walking), while the opposite conditions promote convergence to the static equilibrium.

In summary, the system can exhibit multiple qualitative behaviors, with their respective basins of attraction shaped by both initial conditions and physical parameters. Understanding these interactions is key for designing passive dynamic walkers capable of robust and stable locomotion.